IKKα inactivation promotes Kras-initiated lung adenocarcinoma development through disrupting major redox regulatory pathways

Na-Young Song[a], Feng Zhu[a], Zining Wang[b], Jami Willette-Brown[a], Sichuan Xi[c], Zhonghe Sun[d], Ling Su[d], Xiaolin Wu[d], Buyong Ma[e], Ruth Nussinov[e], Xiaojun Xia[b], David S. Schrump[c], Peter F. Johnson[f], Michael Karin[g,1], and Yinling Hu[a,1]

[a]Cancer and Inflammation Program, Center for Cancer Research, National Cancer Institute, National Institutes of Health, Frederick, MD 21702; [b]State Key Laboratory of Oncology in South China, Collaborative Innovation Center for Cancer Medicine, Sun Yat-Sen University Cancer Center, Guangzhou 510060, China; [c]Thoracic and Gastrointestinal Oncology Branch, Center for Cancer Research, National Cancer Institute, Bethesda, MD 20892; [d]Laboratory of Molecular Technology, Frederick National Laboratory for Cancer Research, Leidos Biomedical Research, Inc., Frederick, MD 21702; [e]Cancer and Inflammation Program, Frederick National Laboratory for Cancer Research, Leidos Biomedical Research, Inc., Frederick, MD 21702; [f]Mouse Cancer Genetics Program, Center for Cancer Research, National Cancer Institute, National Institutes of Health, Frederick, MD 21702; and [g]Department of Pharmacology, University of California, San Diego, La Jolla, CA 92093

Lung adenocarcinoma (ADC) and squamous cell carcinoma (SCC) are two distinct and predominant types of human lung cancer. IκB kinase α (IKKα) has been shown to suppress lung SCC development, but its role in ADC is unknown. We found inactivating mutations and homologous or hemizygous deletions in the *CHUK* locus, which encodes IKKα, in human lung ADCs. The *CHUK* deletions significantly reduced the survival time of patients with lung ADCs harboring *KRAS* mutations. In mice, lung-specific *Ikkα* ablation (*Ikkα^{ΔLu}*) induces spontaneous ADCs and promotes Kras^{G12D}-initiated ADC development, accompanied by increased cell proliferation, decreased cell senescence, and reactive oxygen species (ROS) accumulation. IKKα deletion up-regulates NOX2 and down-regulates NRF2, leading to ROS accumulation and blockade of cell senescence induction, which together accelerate ADC development. Pharmacologic inhibition of NADPH oxidase or ROS impairs Kras^{G12D}-mediated ADC development in *Ikkα^{ΔLu}* mice. Therefore, IKKα modulates lung ADC development by controlling redox regulatory pathways. This study demonstrates that IKKα functions as a suppressor of lung ADC in human and mice through a unique mechanism that regulates tumor cell-associated ROS metabolism.

lung adenocarcinoma | IKKα | ROS | cell senescence | tumor progression

Multiple somatic aberrations in human cancer challenge our understanding of the mechanisms underlying cancer initiation, progression, and metastasis (1, 2). Alterations in secondary tumor drivers and modifiers can diversify signaling pathways, which modulate cancer cell fate as well as therapeutic efficacy. Human lung cancer is the leading cause of cancer-related mortality (3). Human lung cancer is classified into small cell lung cancer (∼15%) and non-small cell lung cancer (NSCLC; ∼85%). Lung squamous cell carcinoma (SCC; 25%) and adenocarcinoma (ADC; 65%) are the main types of NSCLC. Due to a decline in the smoking population, lung ADC has emerged as the predominant lung malignancy in humans. ADC is frequently located in the lower lobes of the lungs or peripheral lung tissues and is derived from type I and II lung epithelial cells (4). SCC is located in the upper lungs and is derived from the basal cells of the bronchial epithelium, and it specifically expresses keratin 5 (K5) and K14 basal cell markers (5). Understanding how these different cancer-associated genetic alterations regulate lung tumorigenesis is important for the design of rational treatments.

Human cancer genome sequencing identifies activating *KRAS* mutations in ∼35% of lung ADC and 5% of lung SCC, and mutations of the gene encoding Kelch-like ECH-associated protein 1 (KEAP1), an E3 ubiquitin ligase that induces degradation of nuclear factor (erythroid-derived 2)-like 2 (NRF2), in 18% and 12% of lung ADC and SCC, respectively (1, 2). *KEAP1* mutations can result in NRF2 accumulation and antioxidant responses (6). In addition, oncogenic Kras and Myc induce NRF2 expression, and the PI3K-AKT signaling activates NRF2 (7). The increased NRF2 exerts its oncogenic potential by enhancing AP-1 and Adam10/EGFR activities and protecting cancer cells from reactive oxygen species (ROS)-induced death (8–10).

The IκB kinase (IKK) complex, composed of IKKα, IKKβ, and NEMO (IKKγ), is essential for the activation of NF-κB and other important cellular functions (11). IKKα regulates canonical and noncanonical NF-κB signaling as well as NF-κB–independent functions (12–15). KEAP1 also regulates turnover of IKKβ, but not of IKKα or NEMO (16). NF-κB activity is required for Kras-initiated lung ADC development because it supports cell survival (17), and an absence of IKKβ attenuates Kras-induced ADC development (18). We have previously shown that lung IKKα inactivation induces spontaneous SCC development in mice, associated with increased lung inflammation (5); however, the role of IKKα in lung ADC is unclear.

Significance

Reactive oxygen species (ROS) can promote tumorigenesis or kill cancer cells. How different cancer-associated genetic alterations regulate ROS balance and outcome is of great importance for the design of rational cancer treatments, many of which affect ROS metabolism and sensing. Kras activation induces a ROS defense system and cell senescence, which counteract its oncogenic activity. *KRAS*-activating mutations are accompanied by IKKα loss mutations that result in elevated NOX2 but decreased expression of the NRF2 ROS defense system. Thus, IKKα ablation turns the antitumorigenic effect of Kras-induced ROS to a protumorigenic effect that enhances Kras-induced progression of lung adenocarcinoma (ADC). Restoration of IKKα activity or inhibition of the pathways activated on its loss may offer new opportunities for ADC treatment.

ROS are essential for maintaining cellular metabolism, survival, proliferation, and differentiation in normal cells. Cancer cells adapt to exist with elevated ROS levels compared with normal cells (19, 20). Numerous studies have documented that excessive ROS either promote tumor development or kill cancer cells via an apoptotic mechanism (21, 22). In response to ROS, NRF2 up-regulates the expression of antioxidants and detoxifying enzymes, thereby maintaining ROS homeostasis. NRF2 has been shown to inhibit Kras^{G12D}-initiated early lung ADC but to accelerate advanced ADC (23); however, most human lung ADCs do not harbor *KEAP1* mutations that result in NRF2 accumulation (1, 24). Thus, there remains a need to identify additional NRF2 regulators and mechanisms underlying NRF2 accumulation or down-regulation in lung ADC.

Chemical carcinogens induce activating *Hras* mutations and ROS accumulation in mouse skin (25, 26). Deletion of NRF2 or NAD(P)H quinone dehydrogenase 1 (NQO1, an NRF2 target) enhances carcinogen-induced skin carcinogenesis in mice (27, 28). *Ikka$^{+/−}$* mice develop many more skin papillomas and malignant carcinomas than wild-type (WT) mice in response to carcinogen administration (26). Given the known activities of NRF2 and NQO1 in scavenging ROS, these phenotypic similarities among NRF2, NQO1, and IKKα suggest that all may impact ROS accumulation and Hras activation during skin tumorigenesis. To date, the regulatory relationship between NRF2 and IKKα remains unclear. Moreover, activated Kras promotes ROS accumulation, which induces cell senescence (29–31), antagonizing Kras-initiated lung ADC progression. How NRF2 regulates the antitumorigenic effects of Kras-induced ROS merits further investigation.

The Cancer Genome Atlas (TCGA) database analysis has revealed the mutations and deletions in the *CHUK* locus, which encodes IKKα, in a subfraction of human lung ADC. Here we show that lung-specific IKKα ablation induces spontaneous lung ADC and promotes Kras-initiated lung ADC development in mice, and further demonstrate that IKKα controls ADC development through its unique effects on ROS metabolism, mediated through NRF2 and NOX2.

Results

Lung Epithelial Cell IKKα Suppresses ADC Development.
To investigate the effect of IKKα on lung ADC development, we ablated IKKα in lungs of C57BL/6 *Ikka$^{f/f}$* mice (15) by intratracheal Adenovirus.Cre (Ad.Cre) administration (*Ikka^{ΔLu}*). Conditional deletion of IKKα resulted in spontaneous lung ADCs in 8 out of 48 *Ikka^{ΔLu}* mice at 13–20 mo of age (Fig. 1*A*, *Top*). No lung ADCs were detected in 30 WT mice. Activating *KRAS* mutations at amino acid 12 are commonly identified in human lung ADC (1), and Kras^{G12D} activation induces spontaneous lung ADC in mice (32). Thus, ADC developed from C57BL/6 *Kras$^{LSL-G12D}$* (*Kras^{G12D}*) mice were used as positive controls (Fig. 1*A*, *Bottom*). With increasing age, ADC derived from *Ikka^{ΔLu}* mice metastasized to the spleen and other organs, as indicated by positivity for SP-C, a marker of type II lung epithelial cells (Fig. S1*A*).

To investigate the effect of IKKα on Kras^{G12D}-induced lung ADC, we crossed C57BL/6 *Ikka$^{f/f}$* mice or *Ikka$^{KA/KA}$* mice with C57BL/6 *Kras^{G12D}* mice and used Ad.Cre to induce Kras^{G12D} expression and simultaneously delete IKKα. *Kras^{G12D};Ikka^{ΔLu}* and *Kras^{G12D};Ikka$^{KA/KA}$* mice showed a significantly greater lung tumor burden compared with *Kras^{G12D}* mice (Fig. 1 *B* and *C* and Fig. S1*B*). ADCs derived from *Kras^{G12D}*, *Kras^{G12D};Ikka^{ΔLu}*, and *Kras^{G12D};Ikka$^{KA/KA}$* mice were positive for SP-C and CC10 (a marker of lung epithelial Clara cells), but negative for K5, an SCC marker (Fig. 1 *D* and *E*). We confirmed *Ikka* deletion and Kras^{G12D} activation in *Kras^{G12D};Ikka^{ΔLu}* lung ADCs and Kras^{G12D} activation in *Kras^{G12D};Ikka$^{KA/KA}$* ADCs (Fig. S1*C*).

Following Ad.Cre treatment, *Kras^{G12D};Ikka$^{f/f}$*, *Kras^{G12D};Ikka$^{f/+}$*, and *Kras^{G12D};Ikka$^{+/−}$* mice showed a significantly reduced life span compared with *Kras^{G12D}* mice (Fig. 1*F* and Fig. S1*D*). Loss of the WT *Ikka* allele [i.e., loss of heterozygosity (LOH), a tumor-suppressor hallmark] was detected in *Kras^{G12D};Ikka$^{+/−}$* lung ADCs (Fig. S1*E*). *Ikka* LOH was previously reported in carcinogen-induced skin tumors in *Ikka$^{+/−}$* mice (26). Collectively, these results indicate that lung epithelial cell IKKα ablation promotes Kras^{G12D}-initiated lung ADC development. Although FVB $_L$-Ikka$^{KA/KA}$ mice, in which lysine is replaced by alanine at amino acid 44 of IKKα, develop spontaneous lung SCC (5), we did not detect lung SCC in FVB or C57BL/6 *Ikka^{ΔLu}* mice, *Kras^{G12D};Ikka^{ΔLu}* mice, or *Kras^{G12D};Ikka$^{KA/KA}$* mice in this study.

We then examined the TCGA database (cBioPortal) of Human Cancer Genomics (1) and found a 2.2% mutation rate in the *CHUK* locus in lung ADC, including *CHUK^{X411}* and *CHUK^{E53}* point mutations, which generate the C-terminal truncated IKKα variants lacking its leucine zipper (LZ) and helix-loop-helix (HLH) domains, as well as *CHUK* homozygous deletions (Fig. 1*G*, *Top*). We also found *CHUK* hemizygous deletions in ~22% of human lung ADCs (Fig. 1*G*, *Bottom*). The LZ and HLH motifs are required for IKKα activity (13, 15, 33, 34). Human lung ADCs carrying *CHUK* mutations had an activating *KRAS* mutation that causes an amino acid change at position 12, as well as *TP53* mutations (Fig. 1*G*, *Top* and Fig. S1*F*). Eight out of 51 human lung ADCs bearing a *CHUK* hemizygous deletion also had an activating *KRAS* G12C or G12V mutation (Fig. 1*G*, *Bottom*), suggesting that some *CHUK* alterations have a positive correlation with activating *KRAS* mutations.

We also examined the effect of *CHUK* mutations on the survival of patients with lung ADC. The median survival of the patients in this cohort is 44.6 mo (1), compared with 19.5 mo for patients with *CHUK* mutations and 35.5 mo for patients with *KRAS* mutations. Although the number of patients with a *CHUK* mutation is limited, the data suggest that patients with lung ADC with *CHUK* mutations may have a tendency toward shorter survival. We further compared the survival curves among patients with *CHUK* alterations, including mutations and hemizygous deletions, *KRAS* mutations, and *KRAS* mutations/*CHUK* hemizygous deletions, and found that *CHUK* mutations or hemizygous deletions significantly reduced the survival time of patients with lung ADC carrying a *KRAS* mutation (Fig. 1*H*). Based on the foregoing animal results, IKKα inactivation may promote human lung ADC development.

Reduced IKKα Promotes Bronchial Epithelial Cell Proliferation and Attenuates Cell Senescence.
Compared with *Kras^{G12D}* mice, *Kras^{G12D};Ikka^{ΔLu}* and *Kras^{G12D};Ikka$^{KA/KA}$* mice developed significantly enlarged lungs with markedly increased Ki67-positive bronchial epithelial cells, which can give rise to lung ADCs (Fig. 2 *A* and *B* and Fig. S2*A*), suggesting that IKKα reduction or deletion promotes lung epithelial cell proliferation. The *Ikka^{KA}* mutation severely destabilizes IKKα and also abolishes its catalytic activity (5). Indeed, IKKα levels were decreased in *Kras^{G12D};Ikka$^{KA/KA}$* lung ADCs compared with WT lungs and *Kras^{G12D}* ADCs (Fig. S2*B*). Moreover, following intratracheal treatment with Ad.Cre, a small group of *Kras^{G12D};Ikka$^{KA/KA}$* mice developed severe skin lesions, precluding their maintenance. Thus, we used *Ikka$^{f/f}$* mice for all subsequent studies.

Oncogenic Kras^{G12D} induces premalignant lesions by increasing cell senescence, as indicated by senescence-associated β-galactosidase (SA-β-gal) staining (30). *Kras^{G12D};Ikka^{ΔLu}* lung ADCs displayed substantially less SA-β-gal staining and more Ki67 than *Kras^{G12D}* ADCs (Fig. 2*C* and Fig. S2*C*). The tumor suppressor p53 is essential for induction of cell senescence (30). Decreased p53 and p21^{Cip1} (p21) expression can overcome cell
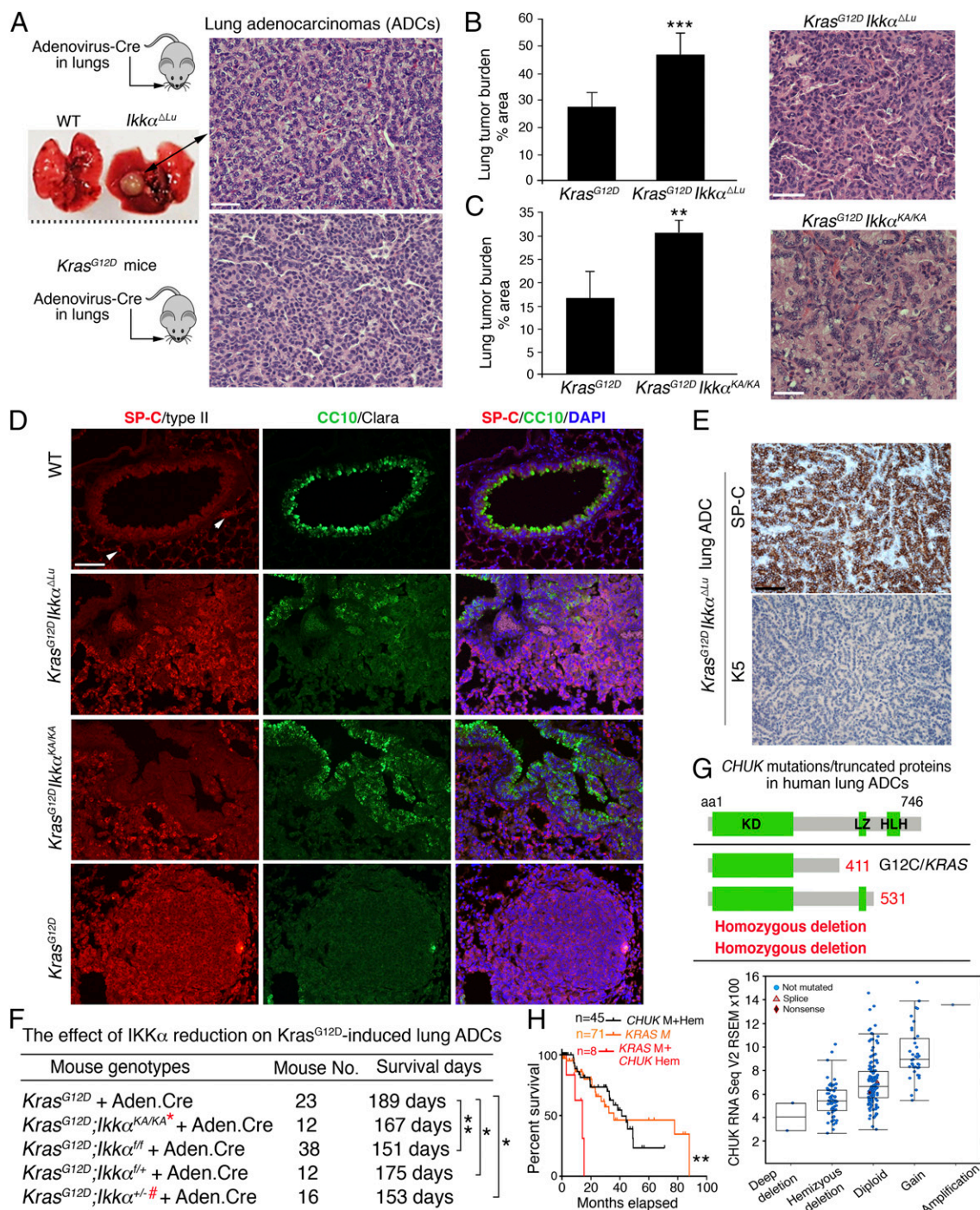
Fig. 1. IKKα deletion induces spontaneous lung ADCs and promotes Kras-initiated lung ADCs, and somatic *CHUK* aberrations are detected in human lung ADCs. (*A, Top*) Lung-specific IKKα ablation by intratracheal Ad.Cre injection induced spontaneous lung ADCs in 8 of 48 *Ikkα*^{ΔLu} mice and in 0 of 30 WT mice. ADCs stained with hematoxylin and eosin (H&E) in *Ikkα*^{ΔLu} mice at age 13 mo. (*A, Bottom*) H&E-stained ADCs from *Kras*^{G12D} mice served as a positive control. (Scale bar: 30 μm.) All images in this study were captured by a Nikon (Ver. 3.06) microscope. (*B*) Lung ADC burden in *Kras*^{G12D} and *Kras*^{G12D};*Ikkα*^{ΔLu} mice at 4 mo after Ad.Cre treatment (*n* = 6 mice/group) and a representative H&E-stained ADC. ***P < 0.001, Student's *t* test. (Scale bar: 25 μm.) (*C*) Lung ADC burden in *Kras*^{G12D} and *Kras*^{G12D};*Ikkα*$^{KA/KA}$ mice at 4.5 mo after Ad.Cre treatment (*n* = 4 mice/group) and a representative H&E-stained ADC. **P < 0.01, Student's *t* test. (Scale bar: 25 μm.) (*D*) Immunofluorescence (IF) staining with anti–SP-C or anti–CC10 antibody showing the tissue origins of ADCs in *Kras*^{G12D}, *Kras*^{G12D};*Ikkα*^{ΔLu}, and *Kras*^{G12D};*Ikkα*$^{KA/KA}$ mice and WT lungs (*n* = 3 mice/group). DAPI, nuclear staining. (Scale bar: 30 μm.) (*E*) ADCs from *Kras*^{G12D};*Ikkα*^{ΔLu} mice were stained by immunohistochemistry (IHC) with K5 or SP-C antibody (*n* = 3). (Scale bar: 30 μm.) (*F*) Survival of *Kras*^{G12D} mice compared with several IKKα mutants crossed with *Kras*^{G12D} mice. **P < 0.01; *P < 0.05, Mantel–Cox log-rank test. Mouse numbers and *P* values are shown. The red asterisk indicates IKKα reduction; the red #, LOH. (*G, Top*) *CHUK* mutations and deletion were found in 230 human lung ADCs (cBioPortal for Cancer Genomics) (1) that generate truncated IKKα proteins labeled with red numbers. aa, amino acid; HLH, helix-loop-helix; KD, kinase domain; LZ, leucine zipper. (*G, Bottom*) Analysis of CHUK (IKKα) mRNA expression (RNA sequence V2 RSEM) in 230 human lung ADCs (1). Putative copy number calls on 230 cases were determined using GISTIC 2.0. Values: −2, homozygous deletion; −1, hemizygous (shallow) deletion; 0, neutral/no change; 1, gain; 2, high-level amplification. (*H*) Survival curves for patients with *CHUK* alterations, including mutations (M) and hemizygous deletions (Hem), *KRAS* mutations, and *KRAS* mutations/*CHUK* hemizygous deletions. **P < 0.01, χ^2 test (comparisons between two groups).
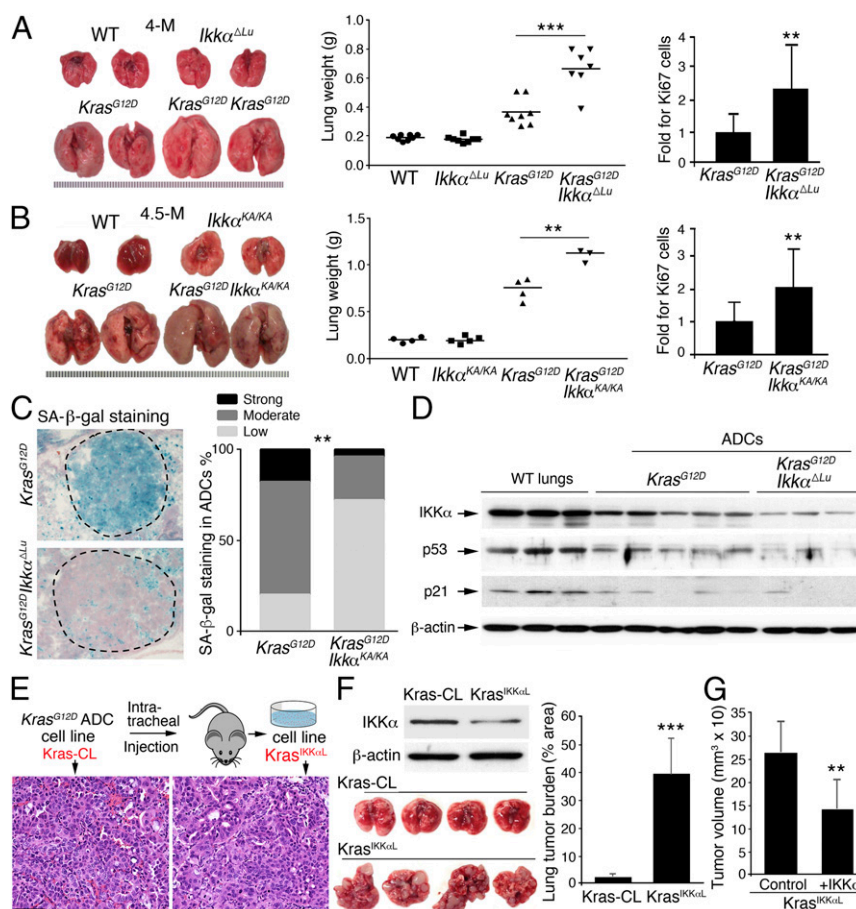
Fig. 2. IKKα deletion promotes cell growth but reduces cell senescence. (*A*) Lung appearance and weights of *Kras^G12D* mice (*n* = 8) and *Kras^G12D;Ikkα^ΔLu* mice (*n* = 7) and Ki67-stained bronchial epithelial cells in the lungs of these mice (*n* = 3 mice for 10 slides/group; *Right*) at 4 mo after Ad.Cre treatment. **P < 0.01; ***P < 0.001, Student's *t* test. (*B*) Lung appearance and weight in four *Kras^G12D* and three *Kras^G12D;Ikkα^KA/KA* mice (*Left* and *Center*) and Ki67-stained bronchial epithelial cells in the lungs of these mice (*n* = 3 mice/group; *Right*) at 4.5 mo after Ad.Cre treatment. **P < 0.01, Student's *t* test. (*C*) Comparison of SA-β-gal staining intensities between *Kras^G12D;Ikkα^ΔLu* and *Kras^G12D* tumors (*n* = 3 mice/group). SA, senescence-associated. **P < 0.01, Fisher's exact test. (*D*) IB analysis of IKKα, p53, and p21 expression in WT lungs and *Kras^G12D* and *Kras^G12D;Ikkα^ΔLu* ADCs. β-actin served as a protein-loading control. (*E*) A scheme for generating Kras-CL and Kras^IKKαL cell lines involving intratracheal injections of these cells into WT mice with a C57BL/6 background. ADCs generated by these cells are stained with H&E. (Scale bar: 25 μm.) (*F*) IB analysis of IKKα in Kras-CL and Kras^IKKαL cells. β-actin served as a protein-loading control (*Top Left*). Shown are lung appearance (*Bottom Left*) and tumor burden (*Right*) in WT mice receiving intratracheal injections of Kras-CL (*n* = 4) or Kras^IKKαL (*n* = 5) cells (5 × 10^6 cells/mouse), as analyzed statistically using Student's *t* test. ***P < 0.001. (*G*) The growth of tumors in nude mice receiving s.c. injection of IKKα- or control vector-transfected Kras^IKKαL cells (*n* = 5 mice/group) for 2 wk. Data represent mean ± SD. **P < 0.01, Student's *t* test.

cycle arrest and senescence and thereby promote tumor progression. Immunoblot (IB) analysis showed lower expression of p53 and p21 in *Kras^G12D;Ikkα^ΔLu* tumors than in *Kras^G12D* tumors (Fig. 2*D*), which may account for the hyperproliferative phenotype in the lungs of *Kras^G12D;Ikkα^ΔLu* mice compared with *Kras^G12D* mice. Of note, decreased IKKα expression was seen in some *Kras^G12D*-lung ADCs and this was accompanied by reduced p53 and p21 expression (Fig. 2*D*). These results suggest that reduced IKKα expression in lung ADCs is associated with increased cell proliferation and decreased cell senescence.

To determine the epithelial cell-autonomous role of IKKα in lung ADC development, we generated a *Kras^G12D* ADC (Kras-CL) cell line (Fig. 2*E*) and transplanted these cells into the lungs of C57BL/6 WT mice. From the resulting lung ADCs, we isolated another cell line, Kras^IKKαL, that expressed less IKKα than the parental Kras-CL cells (Fig. 2*E* and Fig. 2*F*, *Top Left*). Kras^IKKαL cells generated many more ADCs than the parental Kras-CL cells after transplantation into C57BL/6 WT mice, although both cell lines contained an activated Kras^G12D allele (Fig. 2*F*, *Bottom Left* and *Right* and Fig. S2*D*). To verify the inhibitory effect of IKKα on tumorigenesis, we reexpressed IKKα

into Kras^IKKαL cells and found that reintroduction of IKKα reduced tumor sizes compared with controls when these cells were injected s.c. into nude mice (Fig. 2*G* and Fig. S2*E*). These results indicate that reduced IKKα expression in lung ADC cells promotes tumorigenesis.

IKKα Ablation Enhances ROS in Lung ADCs, and Treatment with Apocynin Attenuates ROS and Lung Tumorigenesis. ROS induce p53 expression (35). Unexpectedly, however, we detected more ROS in *Kras^G12D;Ikkα^ΔLu* ADCs than in *Kras^G12D* ADCs (Fig. 3*A*). Using gene expression array analysis (GSE84159), we found increased expression of genes encoding the NADPH oxidase (NOX) complex subunits that are involved in ROS generation (36), such as Cyba, Ncf2, Ncf1, and Cybb, which encodes NOX2 (37), in *Kras^G12D;Ikkα^ΔLu* lungs compared with *Kras^G12D* lungs (Fig. 3*B*). We did not observe increased expression of other NOX types. RT-PCR confirmed the significantly higher levels of Nox2 in *Kras^G12D;Ikkα^ΔLu* lungs compared with *Kras^G12D* lungs (Fig. 3*C*). Moreover, IB analysis showed significantly higher NOX2 levels in *Kras^G12D;Ikkα^ΔLu* ADCs compared with *Kras^G12D* ADCs (Fig. 3*D* and Fig. S3*A*). Indeed, some human
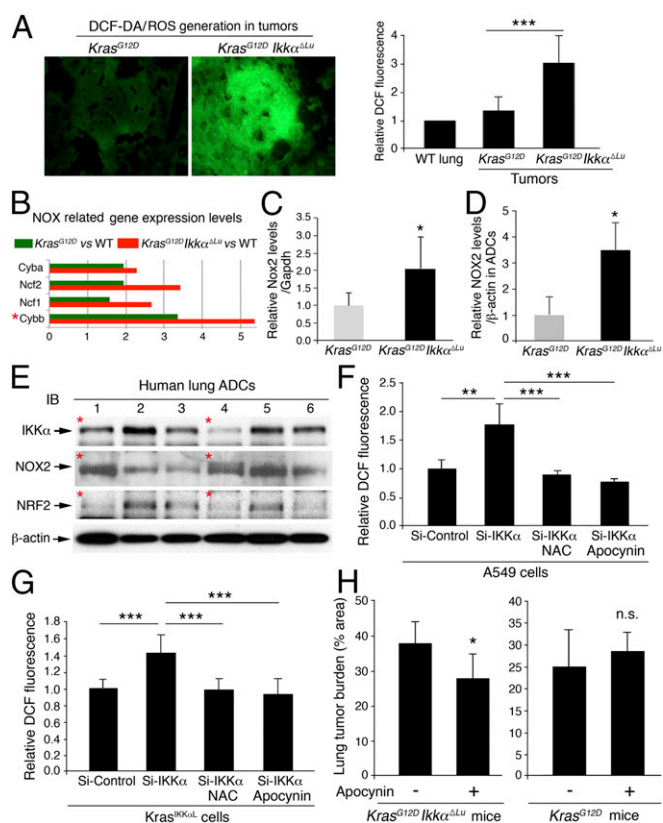
Fig. 3. IKKα ablation increases NOX2 expression, and NOX inhibition reduces lung tumor burden. (*A*) Increased levels of ROS stained with IF (*Left*) for 2′,7′-dichlorofluorescein diacetate (DCF-DA, in green) in tumors derived from $Kras^{G12D};Ikkα^{ΔLu}$ mice compared with $Kras^{G12D}$ tumors and WT lungs (*Right*). n = 6/group. ***$P < 0.001$, Student's *t* test. (*B*) Comparison of expression levels of genes encoding Cyba, Ncf2, Ncf1, and Cybb in $Kras^{G12D};Ikkα^{ΔLu}$ lungs vs. WT (red) and in $Kras^{G12D}$ lungs vs. WT (green), as determined by gene array analysis. Red asterisk: Cybb is also the name of the Nox2 gene. (*C*) RT-PCR analysis of Nox2 mRNA expression in $Kras^{G12D}$ and $Kras^{G12D};Ikkα^{ΔLu}$ lungs (n = 6). Data represent mean ± SEM (three repeats). *$P < 0.05$, Student's *t* test. (*D*) IB analysis of NOX2 expression in four $Kras^{G12D}$ and five $Kras^{G12D};Ikkα^{ΔLu}$ lung ADCs (Fig. S3*A*). Data represent mean ± SD (three repeats). *$P < 0.05$, Student's *t* test. (*E*) IB analysis of IKKα, NOX2, and NRF2 expression in human lung ADCs. Red asterisks indicate a relationship between IKKα and NOX2. β-actin served as a protein-loading control. (*F* and *G*) Apocynin (100 μM) or NAC (10 mM) reduces ROS (stained with DCF-DA) induced by IKKα down-regulation in human A549 cells (*F*) and mouse Kras-CL cells (*G*). (*H*) The effect of apocynin on lung tumor burden in $Kras^{G12D}$ (*Right*) and $Kras^{G12D};Ikkα^{ΔLu}$ (*Left*) mice. n = 6 for untreated mice; n = 9 for treated mice. *$P < 0.05$, Student's *t* test. n.s., not significant.

lung ADCs expressed reduced IKKα and increased NOX2 (Fig. 3*E*). Another analysis (1) showed a negative correlation between NOX2 and IKKα expression in human lung ADCs (Fig. S3*B*), suggesting the relevance of reduced IKKα and increased NOX2 in human lung ADC development.

To verify whether IKKα expression is inversely correlated with ROS in lung ADC, we knocked down IKKα in human A549 lung ADC cells, which carry a $Kras^{G12S}$ mutation (38), and in mouse Kras-CL ADC cells. Down-regulation of IKKα increased ROS in both A549 and Kras-CL cells, but treatment with apocynin, a NOX inhibitor (36), or *N*-acetyl cysteine (NAC), an antioxidant (29), decreased ROS accumulation in IKKα-deficient A549 and Kras-CL cells (Fig. 3 *F* and *G* and Fig. S3 *C* and *D*). Oral administration of apocynin, dissolved in drinking water containing 1.5% ethanol, for 4 mo significantly reduced the lung ADC burden in $Kras^{G12D};Ikkα^{ΔLu}$ mice compared with vehicle-treated

$Kras^{G12D};Ikkα^{ΔLu}$ mice (Fig. 3*H*, *Left*); however, treatment with apocynin did not decrease the lung ADC burden in $Kras^{G12D}$ mice compared with controls (Fig. 3*H*, *Right*). These results suggest that IKKα reduction results in increased amounts of NOX2 and intratumoral ROS. IKKα is part of the IKK complex, but knockdown of IKKα did not alter NF-κB activity in A549 cells (Fig. S3*E*), suggesting that IKKα may regulate NOX2 expression and ROS levels via an NF-κB–independent mechanism.

Knockdown of NOX2 in Lung ADC Cells Inhibits Lung ADC Growth, and IKKα Regulates NOX2 Expression via the *Nox2* Promoter. To verify the relationships among epithelial cell IKKα, NOX2, and ROS in lung tumorigenesis, we confirmed higher ROS levels in Kras[IKKαL] cells than in Kras-CL cells and verified that treatment with apocynin reduced ROS levels in Kras[IKKαL] cells (Fig. 4 *A* and *B*). Because Kras-CL cells required more than 3 mo to generate lung ADCs in WT mice, we used Kras[IKKαL] cells to determine the effect of NOX2 and ROS on ADC formation. Consistently, a 6-wk course of treatment with apocynin reduced Kras[IKKαL] cell–generated lung ADC numbers and lung weights in C56BL/6 WT mice compared with controls (Fig. 4*C*). These results demonstrate that IKKα levels in lung ADC cells are inversely correlated with ROS levels and lung tumor development and that increased ROS enhance the tumorigenic potential of Kras[IKKαL] cells.

Furthermore, Kras[IKKαL] cells expressed higher levels of Nox2 mRNA compared with Kras-CL cells (Fig. 4*D*), and silencing IKKα resulted in elevated NOX2 expression in A549 cells (Fig. S4 *A* and *B*). In contrast, knockdown of NOX2 significantly attenuated ROS levels in Kras[IKKαL] cells and impaired Kras[IKKαL] cell-generated lung tumors in C57BL/6 WT mice at 6 wk after the transplantation of Nox2 Si-RNA– or control Si-RNA–treated Kras[IKKαL] cells (Fig. 4 *E* and *F*), although NOX2 knockdown had less effect on lung weight than apocynin, suggesting that increased NOX2 expression enhances the tumorigenic potential of Kras[IKKαL] cells by elevating ROS levels.

We then investigated the mechanism underlying the regulation of NOX2 expression by IKKα. The aryl hydrocarbon receptor (AhR) is known to repress *Nox2* transcription (39). We postulated that IKKα may regulate *Nox2* transcription via its effects on AhR activity. Indeed, an interaction between IKKα and AhR was detected by pull-down assays with an anti-AhR or an anti-IKKα antibody in A549 cells (Fig. S4*C*). In addition, kinase-inactive IKKα (IKKα-KA), but not a mutant IKKα with its LZ deletion from amino acids 441–531 (IKKα-ΔLZ), interacted with AhR (Fig. S4*D*), suggesting that IKKα may regulate Nox2 expression independent of its kinase activity. Chromatin immunoprecipitation (ChIP) assays demonstrated that both IKKα and AhR were associated with the xenobiotic response element-containing region of the *Nox2* promoter in Kras-CL cells and in human A549 cells (Fig. 4*G* and Fig. S4 *E* and *F*). In contrast, IKKα depletion decreased the recruitment of AhR to the *Nox2* promoter, and reintroduction of WT IKKα or IKKα-KA, but not of IKKα-ΔLZ, recruited AhR to the *Nox2* promoter in IKKα-deficient Kras-CL and A549 cells (Fig. 4*G* and Fig. S4*E*, *Left*, and Fig. S4*F*). Furthermore, silencing IKKα elevated Nox2 expression in Kras-CL cells, while reintroducing IKKα or IKKα-KA, but not IKKα-ΔLZ, elevated NOX2 expression in IKKα-deficient Kras-CL cells (Fig. 4*H* and Fig. S4*E*, *Right*), although a slight reduction in IKKα-KA binding to the *Nox2* promoter was seen, suggesting that IKKα integrity, but not its kinase activity, is required for the regulation of NOX2 expression. These results indicate that IKKα suppresses NOX2 expression by recruiting AhR to the *Nox2* promoter, whereas IKKα deletion diminishes AhR binding to the *Nox2* promoter, leading to increased Nox2 expression and ROS production (Fig. 4*I*).
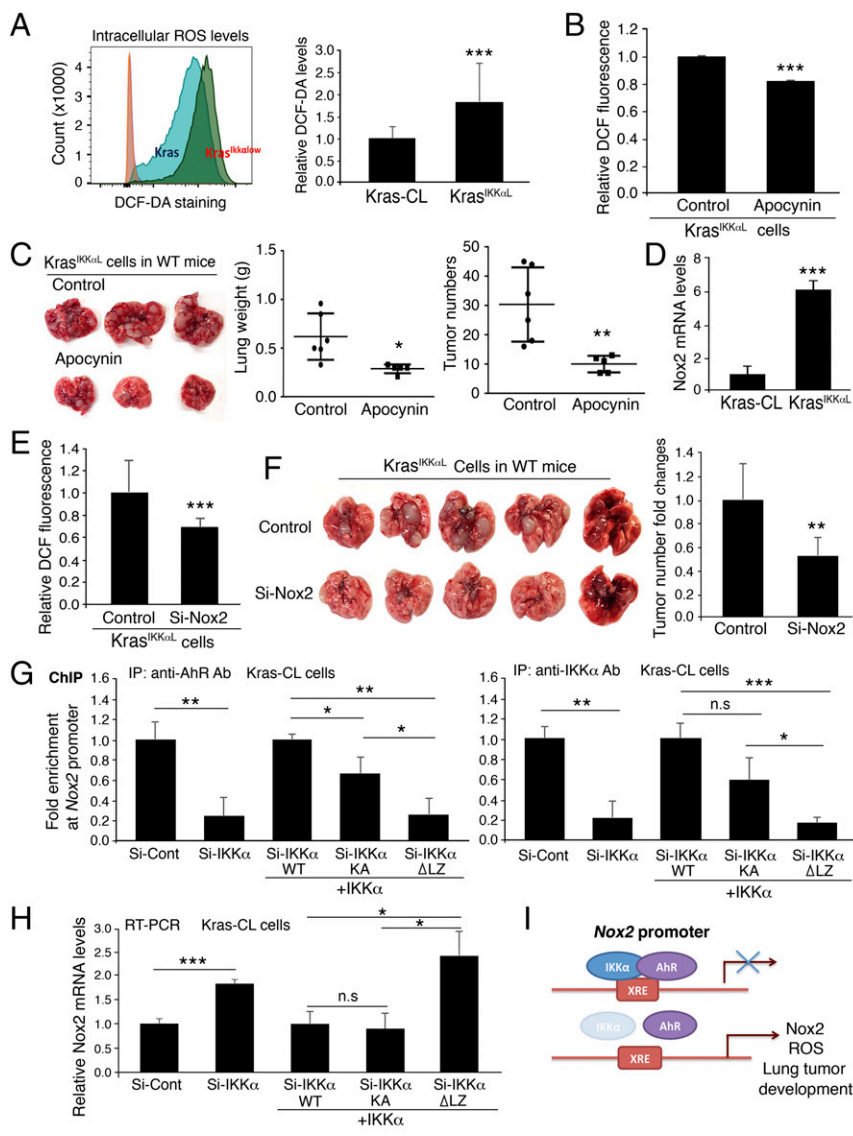
Fig. 4. IKKα represses expression of Nox2 through regulation of AhR activity. (*A, Left*) DCF-DA staining for ROS in Kras-CL (Kras) and Kras^{IKKαL} (Kras^{IKKαlow}) cells using flow cytometry. (*A, Right*) Relative DCF levels in the two cell lines (*n* = 4/group). Data represent mean ± SD (three repeats). ***P < 0.001, Student's *t* test. (*B*) Treatment with apocynin (100 µM) reduces ROS in Kras^{IKKαL} cells (*n* = 3/group). Data represent mean ± SD (three repeats). ***P < 0.001, Student's *t* test. (*C*) Treatment with apocynin inhibits Kras^{IKKαL} cell-derived lung ADCs and reduces lung size in WT mice compared with the untreated control group. Experimental mice, *n* = 5; control mice, *n* = 6. *P < 0.05; **P < 0.01, Student's *t* test. (*D*) RT-PCR analysis of Nox2 mRNA expression in Kras-CL and Kras^{IKKαL} cells (*n* = 3). Data represent mean ± SD (three repeats). ***P < 0.001, Student's *t* test. (*E*) DCF-DA levels of Kras^{IKKαL} cells treated with Si-control (control) or Si-Nox2. *n* = 3/group. Data represent mean ± SD (three repeats). ***P < 0.001, Student's *t* test. (*F*) Tumor appearance (*Left*) and numbers (*Right*) generated by Kras^{IKKαL} cell receiving Si-control and Si-Nox2 RNA in the lungs of WT mice. *n* = 5 for controls; *n* = 6 for Si-Nox2). Data represent mean ± SD **P < 0.01; Student's *t* test. (*G*) ChIP analyses for IKKα and AhR binding to Nox2 promoter using antibody against AhR (*Left*) or IKKα (*Right*) for IP, followed by PCR with Nox2 promoter primers in Kras-CL cells (Si-Cont, control) or Kras-CL cells silencing IKKα or overexpressing WT IKKα, IKKα mutant lacking its LZ motif (IKKα-ΔLZ), and IKKα-KA (kinase inactivation). Si-Cont, Si-control RNA; Si-IKKα, Si-IKKα RNA. Data represent mean ± SD (three repeats). *P < 0.05; ***P < 0.001, Student's *t* test. n.s., not significant. (*H*) Knockdown of IKKα (Si-IKKα) or reintroduction of WT IKKα, IKKα-ΔLZ, and IKKα-KA regulates Nox2 expression in Kras-CL cells, as analyzed by RT-PCR. Data represent mean ± SD (three repeats). ***P < 0.001; **P < 0.01, Student's *t* test. n.s., not significant. (*I*) A working model for regulation of Nox2 expression by IKKα through AhR. XRE, xenobiotic response element, a DNA-binding site for AhR on the Nox2 promoter. IKKα deletion reduces AhR binding to the Nox2 promoter, enhancing Nox2 promoter activity and lung tumor development.

Kras^{G12D};Ikkα^{ΔLu} ADCs Express Reduced NRF2, and NAC Treatment Inhibits Lung ADC Burden in Kras^{G12D};Ikkα^{ΔLu} Mice. A feedback loop between ROS production and elimination balances physiological ROS amounts. We expected to find that increased ROS resulted in NRF2 activation. Surprisingly, however, the expression of NRF2 target genes encoding antioxidants and detoxifying enzymes was lower in Kras^{G12D};Ikkα^{ΔLu} lungs than in Kras^{G12D} lungs (Fig. S5*A*). IB analysis showed that Kras^{G12D} ADCs expressed more NRF2 than WT lungs, whereas Kras^{G12D}; Ikkα^{ΔLu} ADCs expressed less NRF2 than WT lungs (Fig. 5*A*). Among Kras^{G12D} ADCs, those expressing less IKKα consistently showed lower NRF2 and p21 expression (Fig. 5*B*). Importantly, IB analysis showed reduced IKKα and NRF2 expression in a subfraction of human lung ADCs, and indeed, some human lung ADCs showed reduced IKKα and NRF2 expression and increased NOX2 expression (Fig. 3*E* and Fig. S5*B*). Moreover, using RT-PCR, we examined additional 47 human lung ADCs (stage II–IV) and found that a subgroup of these ADCs expressed significantly less IKKα and NRF2 compared with another ADC group (Fig. 5*C*), suggesting clinical relevance of the reduced IKKα and NRF2 expression in human lung ADC.

If reduced NRF2 expression promotes ROS accumulation, which further contributes to increased tumorigenesis, then treatment with NAC should inhibit lung ADC burden in Kras^{G12D};Ikkα^{ΔLu} mice. Indeed, NAC treatment significantly decreased lung weights and ADC burden in Kras^{G12D};Ikkα^{ΔLu} mice compared with controls, but this treatment did not significantly affect the ADC burden in Kras^{G12D} mice (Fig. 5 *D* and *E*). The oxidative DNA damage (8-OHdG) marker was higher in Kras^{G12D};Ikkα^{ΔLu} ADCs than in Kras^{G12D} ADCs, and NAC treatment decreased DNA damage (Fig. 5*F*), suggesting that accumulated ROS cause more DNA damage, which is associated with enhanced lung tumorigenesis. As expected, the expression levels of NRF2 targets Nqo1 and Gpx2 were significantly lower in Kras^{G12D};Ikkα^{ΔLu} ADCs than in Kras^{G12D} ADCs (Fig. 5*G*), suggesting that ROS scavengers regulate lung ADC development in the absence of IKKα.

IKKα Loss Down-Regulates NRF2 Expression in an Epigenetic Manner. Treatment with NAC decreased the number of ROS in Kras^{IKKαL} cells and also inhibited Kras^{IKKαL} cell-generated lung tumor growth in WT mice compared with controls (Fig. 6 *A* and *B*), suggesting a reciprocal correlation between IKKα-regulated NRF2 expression and ROS levels during lung tumorigenesis. KEAP1 is a major negative regulator of NRF2 stability (40). Kras-CL and Kras^{IKKαL} cells expressed similar amounts of
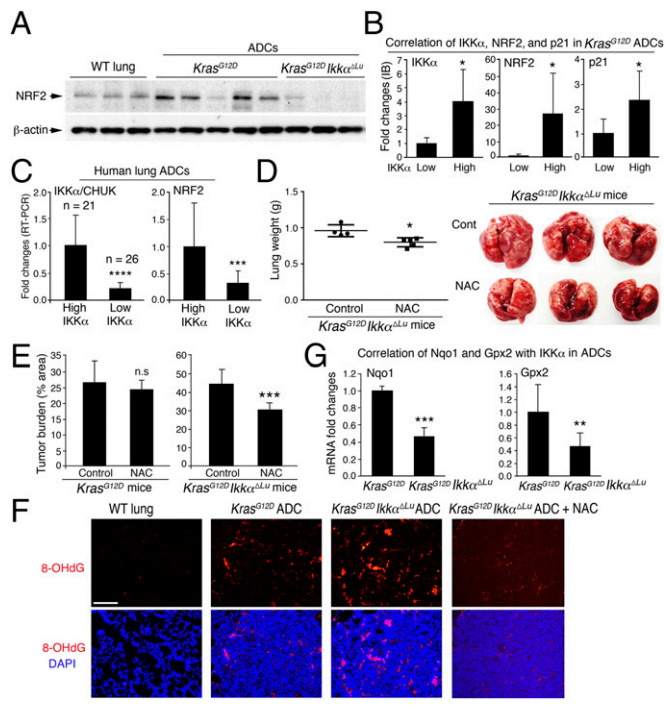
Fig. 5. IKKα ablation reduces NRF2 expression, and inhibition of ROS decreases lung tumorigenesis. (*A*) IB analysis of NRF2 expression in WT lungs and $Kras^{G12D}$ and $Kras^{G12D};Ikka^{\Delta Lu}$ ADCs. β-actin served as a protein-loading control. The same protein membrane was used as shown in Fig. 2*D*. (*B*) IB analysis of expression of IKKα, NRF2, and p21 in $Kras^{G12D}$ ADCs. Based on expression levels of IKKα, these ADCs were divided into two groups: low group ($n = 5$) and high group ($n = 9$). NRF2 and p21 levels were further compared between the two ADC groups and then statistically analyzed using Student's t test. *$P < 0.05$. (*C*) RT-PCR analysis of expression levels of IKKα/CHUK and NRF2 in 47 human lung ADCs. These ADCs were divided into two groups ($n = 21$ and $n = 26$) based on IKKα levels. Gapdh levels were used to normalize IKKα and NRF2 expression. ***$P < 0.001$; ****$P < 0.0001$, Student's t test. (*D*) Lung weight and appearance in $Kras^{G12D};Ikka^{\Delta Lu}$ mice treated with ($n = 5$) or without ($n = 4$) NAC, statistically analyzed by Student's t test. *$P < 0.05$. (*E*) Tumor burden in $Kras^{G12D}$ mice (*Left*) treated with ($n = 4$) or without ($n = 4$) NAC and $Kras^{G12D};Ikka^{\Delta Lu}$ mice (*Right*) treated with ($n = 5$) or without ($n = 4$) NAC. Data were statistically analyzed by Student's t test. n.s., not significant. (*F*) Oxidative DNA damage indicated by IF staining with 8-hydroxy-2′-deoxyguanosine (8-OHdG) in WT lungs and ADCs of $Kras^{G12D}$, $Kras^{G12D};Ikka^{\Delta Lu}$, and NAC-treated $Kras^{G12D};Ikka^{\Delta Lu}$ mice ($n = 5$). (Scale bar: 25 μm.) (*G*) RT-PCR analysis of Nqo1 and Gpx2 mRNA in $Kras^{G12D}$ ($n = 3$) and $Kras^{G12D};Ikka^{\Delta Lu}$ ($n = 4$) lung ADCs. Data were statistically analyzed by Student's t test. **$P < 0.01$; ***$P < 0.001$.

KEAP1, however (Fig. S6*A*). Expression of Nrf2 mRNA was lower in $Kras^{G12D};Ikka^{\Delta Lu}$ lungs than in $Kras^{G12D}$ lungs (Fig. 6*C*). Knockdown of IKKα attenuated NRF2 expression, and reintroduction of IKKα rescued NRF2 expression (Fig. S6*B*), suggesting that IKKα regulates *Nrf2* gene transcription.

Trimethylation at lysine 9 of histone H3 (H3-K9) represses gene expression by recruiting DNA methyltransferases, and trimethyltransferase Suv39h1 is required for H3-K9 trimethylation (13, 41, 42). We previously reported that IKKα interacts directly with H3 protein, which in turn shields chromatin-associated H3 from H3-K9 trimethylation by preventing Suv39h1 from accessing the *Stratifin* chromatin (13). Several CpG islands are present in the *Nrf2* promoter region. Nrf2 mRNA levels were significantly lower in Kras^IKKαL cells than in Kras-CL cells (Fig. 6*D*). Treatment with 5-azacytidine, a DNA methyltransferase inhibitor, increased Nrf2 mRNA levels in Kras^IKKαL cells (Fig. 6*E*), suggesting that IKKα modulates the *Nrf2* promoter activity in an epigenetic manner.

Using ChIP assays, we found IKKα to be associated with the *Nrf2* promoter in Kras-CL cells (Fig. 6*F* and Fig. S6*C*). With the loss of IKKα from the *Nrf2* promoter in Kras^IKKαL cells, increased levels of trimethylated-H3-K9, Suv39h1, and Dnmt3a were found at the *Nrf2* promoter compared with Kras-CL cells (Fig. 6*F* and Fig. S6*C*). Reintroducing WT IKKα or IKKα-KA, but not IKKα-ΔLZ, formed the complex with *Nrf2* promoter in Kras^IKKαL cells (Fig. S6*D*). Consistently, silencing IKKα decreased Nrf2 expression in Kras-CL cells, and reintroducing WT IKKα or IKKα-KA, but not IKKα-ΔLZ, increased Nrf2 expression in IKKα-deficient Kras-CL cells (Fig. 6*G*). These results suggest that IKKα suppresses H3-K9 trimethylation on the *Nrf2* promoter, thereby increasing its transcription. In contrast, IKKα loss elevates H3-K9 trimethylation on the *Nrf2* promoter, inhibiting NRF2 expression (Fig. 6*H* and Fig. S6*E*).

To elucidate how IKKα expression is down-regulated in Kras^IKKαL cells, we sequenced full-length IKKα cDNA and identified a missense mutation at nucleotide 2054 (amino acid 685) in Kras^IKKαL cells, Kras-CL cells, and Kras^G12D-induced ADCs (Fig.
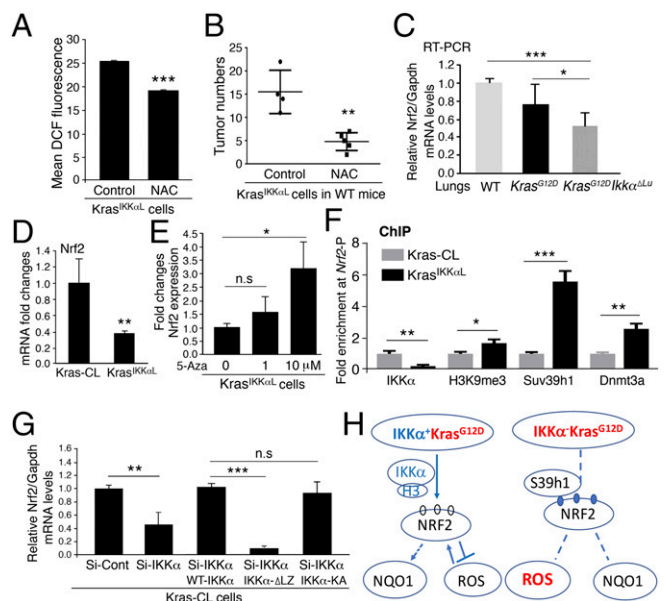

Fig. 6. IKKα regulates NRF2 expression in an epigenetic manner. (*A*) Treatment with NAC (10 mM) inhibits DCF (ROS) levels in Kras^IKKαL cells ($n = 3$/group). Data represent mean ± SD (three repeats). ***$P < 0.001$, Student's t test. (*B*) Treatment with NAC (10 g/L) inhibits the development of lung tumors generated by Kras^IKKαL cells in WT mice. Control mice, $n = 4$; NAC-treated mice, $n = 5$. Data represent mean ± SD. **$P < 0.01$, Student's t test. (*C*) RT-PCR analysis of Nrf2 mRNA levels in four WT, six $Kras^{G12D}$, and 10 $Kras^{G12D};Ikka^{\Delta Lu}$ lungs. Data are analyzed by Student's t test. *$P < 0.05$; ***$P < 0.001$. (*D*) RT-PCR analysis of Nrf2 mRNA in Kras-CL and Kras^IKKαL cells ($n = 3$/group). Data represent mean ± SD (three repeats). **$P < 0.01$, Student's t test. (*E*) RT-PCR analysis of Nrf2 mRNA expression in Kras^IKKαL cells following treatment with 5-azacytidine (5-Aza). Data represent mean ± SD (three repeats). **$P < 0.01$, Student's t test. n.s., not significant. (*F*) ChIP analyses for binding of IKKα, trimethylated-H3K9 (H3K9me3), Suv39h1, or Dnmt3a to *Nrf2* promoter using antibodies against these proteins for immunoprecipitation, followed by PCR with *Nrf2* promoter (-P) primers. Data represent mean ± SD (three repeats). *$P < 0.05$; **$P < 0.01$; ***$P < 0.001$, Student's t test. (*G*) Knockdown of IKKα (Si-IKKα) or reintroduction of WT IKKα, IKKα-ΔLZ, and IKKα-KA regulates Nrf2 expression in Kras-CL cells, as analyzed by RT-PCR. Data represent mean ± SD (three repeats). ***$P < 0.001$; **$P < 0.01$, Student's t test. n.s., not significant. (*H*) A working model for NRF2 regulation and the pathways in IKKα+Kras^G12D and IKKα−Kras^G12D ADC cells. Blue circle, trimethylation; white circle, no trimethylation; S39h1, Suv39h1; H3, histone H3; arrow, promotion; cross lines, inhibition; dashed line, no response; dashed arrow, discussed in Fig. 7.

S6F). Interestingly, Kras^IKKαL cells exhibited many additional *Ikkα* mutations surrounding the nucleotide 2054 genetic lesion, suggesting that these mutations confer a growth advantage, possibly by destabilizing the IKKα protein. Accordingly, IKKα immunoprecipitation from Kras-CL and Kras^IKKαL cells, followed by IB analysis with an anti-ubiquitin antibody, showed more ubiquitinated IKKα in Kras^IKKαL cells compared with Kras-CL cells (Fig. S6G, *Top*). Treatment with MG132, a proteasome inhibitor, elevated IKKα and NRF2 levels in Kras^IKKαL cells (Fig. S6G, *Bottom*), suggesting that tumor-associated mutations promote proteasomal degradation of IKKα. We previously detected the same *Ikkα* mutations and deletions in the C-terminal region of IKKα in skin SCCs derived from carcinogen-treated *Ikkα^+/−* and WT mice (13, 15, 26). These mutations impaired the IKKα activity that controls the G2/M cell cycle checkpoint in response to DNA damage and keratinocyte growth. Thus, the DNA encoding the IKKα C-terminal region behaves like a mutational "hot spot" in different types of cancers.

A ROS-Mediated NRF2-NQO1 Pathway Leads to the Induction of p53/p21 and Cell Senescence, and IKKα Inactivation Reverses This Pathway.

Reduction of NQO1, an NRF2 target, results in p53 degradation independent of MDM2 (43, 44), suggesting that along with antioxidative activity, the ROS-mediated NRF2-NQO1 pathway may prevent tumor progression by up-regulating p53, p21, and cell senescence (30). We hypothesized that reduced IKKα down-regulates NRF2 and NQO1 expression, which attenuates p53 and p21 expression and cell senescence. Indeed, Kras^IKKαL cells expressed reduced IKKα, NRF2, NQO1, p53, and p21 and showed attenuated cell senescence compared with Kras-CL cells (Fig. 7 *A*, *Left* and *B*). Silencing of IKKα repressed NRF2, NQO1, p53, and p21 expression and attenuated cell senescence in Kras-CL and A549 cells (Fig. 7 *A*, *Center* and *C* and Fig. S7 *A* and *B*). In addition, silencing of NRF2 or NQO1 repressed NQO1, p53, and p21 expression and attenuated cell senescence in Kras-CL cells (Fig. 7 *A*, *Right*, *D* and *E* and Fig. S7C). These results suggest that IKKα reduction blocks cell cycle arrest by decreasing NRF2, NQO1, and p21 expression. Importantly, silencing of IKKα, NRF2, or NQO1 in Kras-CL cells promoted tumor growth compared with the control when these cells were injected s.c. into nude mice (Fig. 7 *F–H*).

To demonstrate links among IKKα action, ROS, and ROS-mediated cell senescence, we examined the effect of NAC and apocynin on cell senescence (p53/p21) in Kras^IKKαL and Kras-CL cells (Fig. 7I). Indeed, treatment with NAC or apocynin induced p53/p21 expression in Kras^IKKαL cells. This induction was stronger in Kras^IKKαL cells than in Kras-CL cells (Fig. 7I). Taken together, these findings show that IKKα ablation not only elevates NOX2 expression, but also blocks the induction of NRF2 and NQO1, resulting in accumulated ROS and attenuated cell senescence, both of which promote lung tumor development (Fig. 7J).

Furthermore, we examined NF-κB activity in Kras-CL and Kras^IKKαL cells following TNFα treatment, and found that NF-κB activity was not decreased in Kras^IKKαL cells compared with Kras-CL cells (Fig. S7D). However, relative to Kras-CL, Kras^IKKαL cells showed increased expression of the regulators for stem cell properties, mitogenic activity, and inflammation and reduced expression of the regulators for apoptosis and antioxidant/detoxification functions, as analyzed by a microarray assay (GSE84163; Fig. S7E). Among these alterations, IKKα down-regulates Fgf13, Adam12, and Egfr (14, 15) and ROS elevate Jak2, Egfr, and Notch1 expression (45–47). These changes may also contribute to the enhanced tumorigenic potential of Kras^IKKαL cells compared with Kras-CL cells.

Discussion

Here we demonstrate that lung-specific IKKα deletion promotes Kras^G12D-mediated lung ADC development in association with elevated NOX2, down-regulated NRF2, accumulated ROS, and attenuated cell senescence. Pharmacologic inhibition of NOX or ROS attenuates lung ADC development in Kras^G12D;Ikkα^ΔLU mice. These results define a previously undescribed role of IKKα, in which dual IKKα-NOX2 and IKKα-NRF2 pathways control ROS homeostasis and proliferation/survival that regulate Kras^G12D-mediated lung ADC growth. Importantly, a fraction of human lung ADCs harbor *CHUK* locus mutations and deletions or express reduced IKKα, some of which coexpress activated KRAS. During malignancy development, the activation of oncogenes is a ubiquitous phenomenon. Human lung ADCs express different oncogenes that induce mitogenic stress and ROS (29). Therefore, the mechanism identified in this study may apply in those *CHUK*-deficient human ADCs that do not carry *KRAS* alterations. Furthermore, *KRAS* mutations frequently occur in human pancreatic and colon cancers (cBioPortal). *CHUK* mutations and hemizygous deletions are also found in these patients, suggesting that IKKα inactivation or reduction may promote *KRAS* mutation-involved pancreatic and colon cancer development through a mechanism provided in this study.

FVB L-Ikkα^KA/KA mice develop spontaneous lung SCCs, in which no activating *Kras* mutations are detected, but not ADCs (5). L-Ikkα^KA/KA mice develop systemic inflammation, marked pulmonary macrophage infiltration, and reduced epithelial cell IKKα levels before lung SCC formation. Restoration of IKKα in K5-expressing lung epithelial cells or depleting macrophages prevents lung SCC development. In this study, we detected lung ADCs, but not SCCs, in Kras^G12D, Ikkα^ΔLU, and Kras^G12D; Ikkα^ΔLU mice. These mice have a WT background before Ad.Cre treatment. Furthermore, Kras^G12D;Ikkα^KA/KA mice only developed lung ADCs. Notably, activating *KRAS* mutations are detected in ~35% and 5% of human lung ADCs and SCCs, respectively (1, 2), suggesting that activated Kras may predominantly induce ADCs in the lung, and that inflammatory conditions may also determine the formation of lung cancer, either ADC or SCC (4). The detailed mechanism remains to be revealed. Moreover, lung-specific *Ikkα* ablation induced spontaneous lung ADCs. Reintroduction of IKKα inhibited Kras^IKKαL cell-generated tumor growth, and silencing of IKKα promoted Kras-CL cell-generated tumor growth. Hence, the epithelial-intrinsic IKKα is critical for suppressing lung ADC development.

Down-regulation of NF-κB can cause apoptosis of Kras^G12D ADC cells expressing reduced p53 (17, 18). Here, we showed that Kras^G12D;Ikkα^ΔLU and Kras^G12D ADCs expressed comparable amounts of nuclear NF-κB proteins, although p53 expression was lower in Kras^G12D;Ikkα^ΔLU ADCs than in Kas^G12D ADCs, suggesting that a basal NF-κB activity is sufficient for maintaining tumor cell survival. Furthermore, Kras^G12D;Ikkα^ΔLU ADCs showed increased proliferating cells and reduced p53/p21/senescence. NQO1 has been shown to stabilize the p53 protein independent of MDM2, while reduced NQO1 destabilizes p53 (43, 44). We found that IKKα deletion decreased expression of NRF2 and NQO1, which led to reduced p53/p21 and cell senescence in lung cancer cells, suggesting that IKKα is required to maintain NRF2, NQO1, and p53/p21 pathways for establishment of a barrier that antagonizes tumor progression.

On the other hand, silencing of IKKα was found to down-regulate NRF2 and NQO1 expression, resulting in reduced p53/p21 expression and cell senescence. Therefore, a reduction in IKKα changes the antitumorigenic effect of Kras-induced ROS to a protumorigenic effect that enhances Kras-induced ADC progression. Although it has been reported that NRF2 deletion alone promotes the Kras^G12D-mediated early ADCs and inhibits the advanced Kras^G12D-mediated ADCs (23, 48), in this study, along with reduced NRF2, IKKα deletion also promoted NOX2 expression, leading to further ROS accumulation and oxidative damage. Most likely, the ROS scavenging system induced by NRF2 becomes more
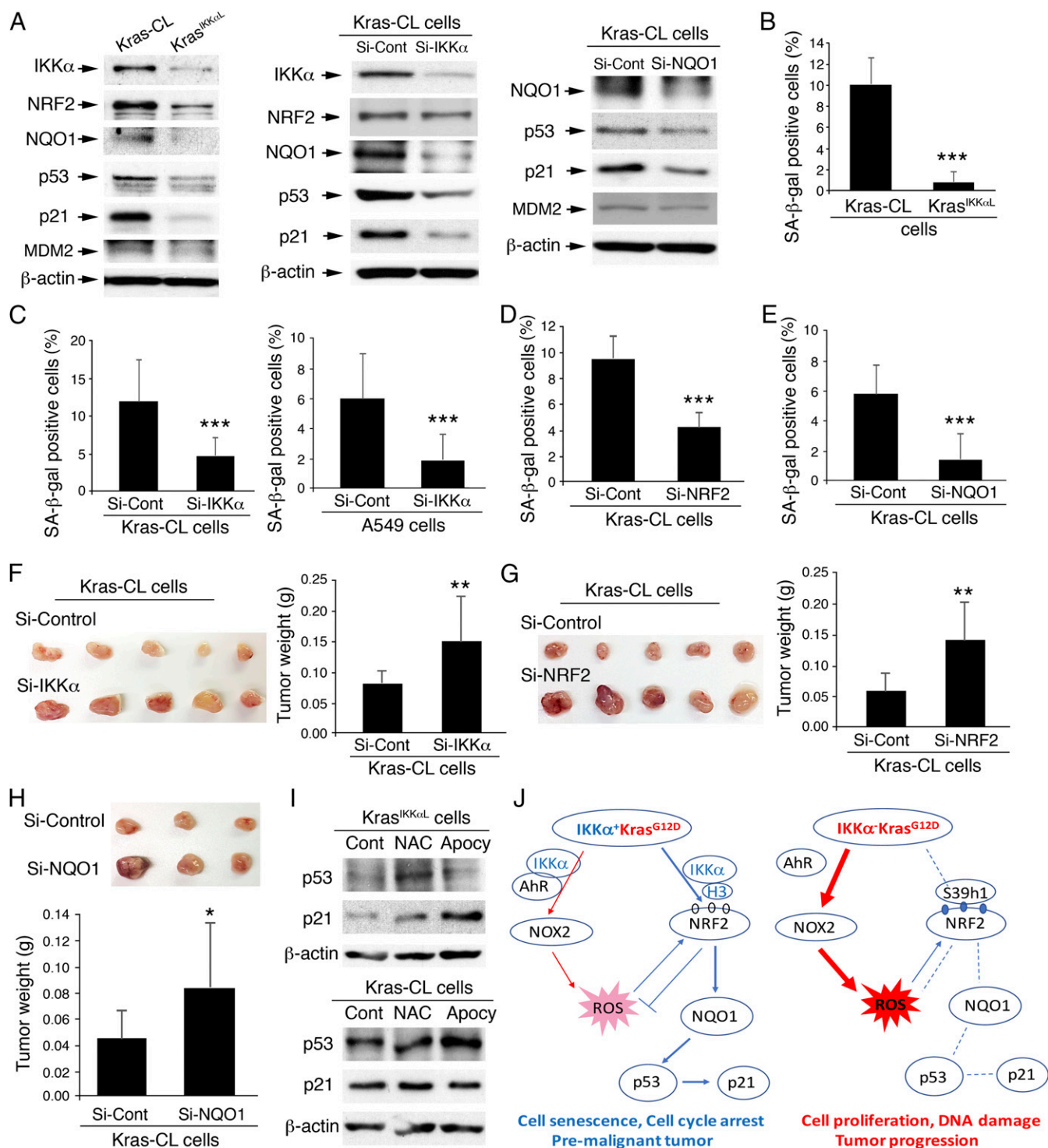
Fig. 7. An antagonizing relationship between accumulating ROS pathways and senescence. (*A*) IB analysis of IKKα, NRF2, NQO1, p53, p21, and MDM2 expression in Kras-CL and Kras^{IKKαL} cells (*Left*), as well as Kras-CL cells treated with Si-Control, Si-IKKα (*Center*), or Si-NQO1 (*Right*). β-actin served as a protein-loading control. (*B*) SA-β-gal–positive cells in Kras-CL and Kras^{IKKαL} cells ($n = 3$/group). Data represent mean ± SD (three repeats). ***$P < 0.001$, Student's t test. (*C*) The effect of IKKα knockdown on SA-β-gal levels in Kras-CL cells (*Left*) and A459 cells (*Right*) ($n = 3$/group). Data represent mean ± SD (three repeats). ***$P < 0.001$, Student's t test. (*D*) The effect of NRF2 knockdown on SA-β-gal levels in Kras-CL cells ($n = 3$/group). Data represent mean ± SD (three repeats). ***$P < 0.001$, Student's t test. (*E*) The effect of NQO1 knockdown on SA-β-gal levels in Kras-CL cells ($n = 3$/group). Data represent mean ± SD (three repeats). ***$P < 0.001$, Student's t test. (*F*) Appearance (*Left*) and weight (*Right*) of tumors in nude mice receiving s.c. injections of Si-control or Si-IKKα–transfected Kras-CL cells for 3 wk ($n = 10$ tumors from 5 mice/group). Data represent mean ± SD. **$P < 0.01$, Student's t test. (*G*) Appearance (*Left*) and weight (*Right*) of tumors in nude mice receiving s.c. injections of Si-control or Si-NRF2–transfected Kras-CL cells for 3 wk ($n = 10$ tumors from 5 mice/group). Data represent mean ± SD. **$P < 0.01$, Student's t test. (*H*) Appearance (*Top*) and weight (*Bottom*) of tumors in nude mice receiving s.c. injections of Si-control or Si-NQO1 transfected Kras-CL cells for 3 wk ($n = 9$ tumors from 5 mice/group). Data represent mean ± SD. *$P < 0.05$, Student's t test. (*I*) IB analysis of p53 and p21 expression in Kras-CL and Kras^{IKKαL} cells treated with NAC or apocynin (Apocy). Cont, untreated cells. β-actin served as a protein-loading control. (*J*) A working model for regulation of NOX2 or NRF2, their pathways, and biological consequences, regulated by IKKα in IKKα$^+$Kras^{G12D} and IKKα$^-$Kras^{G12D} ADC cells. Blue circle, trimethylation; white circle, no trimethylation; S39h1, Suv39h1; H3, histone H3; arrow, promotion or forward/maintaining; cross lines, inhibition; dashed line, no response.

crucial for reducing oxidative damage in $Kras^{G12D};Ikk\alpha^{\Delta LU}$ mice than in $Kras^{G12D}$ mice. Overall, IKKα provides a protective role that suppresses excessive ROS and also ensures a pathway for ROS-induced antitumorigenic activity, thereby preventing ADC initiation and progression.

Materials and Methods

All mice used in this study were cared for in accordance with the guidelines of the Institutional Animal Care and Use Committee (IACUC) of the National Institutes of Health. All animal experiments (protocols 14–051 and 14–052) were approved by the IACUC. $Ikk\alpha^{f/f}$, $Ikk\alpha^{KA/KA}$, and $Ikk\alpha^{+/-}$ mice (12, 13, 15) and $Kras^{G12D}$ mice (stock no. 008179; The Jackson Laboratory) were on a C57BL/6 background. Athymic nude mice were obtained from Charles River Laboratories [BALB/c; Crl:NU(NCr)-Foxn1^{nu}]. Human lung adenocarcinomas were obtained from Dr. David Schrump, Thoracic and Gastrointestinal Oncology Branch, National Cancer Institute and from Sun Yat-Sen University

Cancer Center, Guangzhou, China. All human samples used in this study were approved by the National Institutes of Health Internal Review Board (protocol 06-C-0014) and by the Ethics Committee and Institutional Review Board of Sun Yat-Sen University Cancer Center (YB2017-023), and informed consent was been obtained from all patients.

1. Cancer Genome Atlas Research Network (2014) Comprehensive molecular profiling of lung adenocarcinoma. *Nature* 511:543–550, and erratum (2014) 514:262.
2. Hammerman PS, et al.; Cancer Genome Atlas Research Network (2012) Comprehensive genomic characterization of squamous cell lung cancers. *Nature* 489:519–525, and erratum (2012) 491:288.
3. Larsen JE, Minna JD (2011) Molecular biology of lung cancer: Clinical implications. *Clin Chest Med* 32:703–740.
4. Ji H, et al. (2007) LKB1 modulates lung cancer differentiation and metastasis. *Nature* 448:807–810.
5. Xiao Z, et al. (2013) The pivotal role of IKKα in the development of spontaneous lung squamous cell carcinomas. *Cancer Cell* 23:527–540.
6. Hast BE, et al. (2014) Cancer-derived mutations in KEAP1 impair NRF2 degradation but not ubiquitination. *Cancer Res* 74:808–817.
7. Mitsuishi Y, et al. (2012) Nrf2 redirects glucose and glutamine into anabolic pathways in metabolic reprogramming. *Cancer Cell* 22:66–79.
8. Chio IIC, et al. (2016) NRF2 promotes tumor maintenance by modulating mRNA translation in pancreatic cancer. *Cell* 166:963–976.
9. Umemura A, et al. (2016) p62, up-regulated during preneoplasia, induces hepatocellular carcinogenesis by maintaining survival of stressed HCC-initiating cells. *Cancer Cell* 29:935–948.
10. Juilland M, et al. (2016) CARMA1- and MyD88-dependent activation of Jun/ATF-type AP-1 complexes is a hallmark of ABC diffuse large B-cell lymphomas. *Blood* 127:1780–1789.
11. Ghosh S, Karin M (2002) Missing pieces in the NF-kappaB puzzle. *Cell* 109(Suppl 1):S81–S96.
12. Hu Y, et al. (1999) Abnormal morphogenesis but intact IKK activation in mice lacking the IKKalpha subunit of IkappaB kinase. *Science* 284:316–320.
13. Zhu F, et al. (2007) IKKalpha shields 14-3-3sigma, a G(2)/M cell cycle checkpoint gene, from hypermethylation, preventing its silencing. *Mol Cell* 27:214–227.
14. Xia X, et al. (2013) An IKKα-nucleophosmin axis utilizes inflammatory signaling to promote genome integrity. *Cell Rep* 5:1243–1255.
15. Liu B, et al. (2008) IKKalpha is required to maintain skin homeostasis and prevent skin cancer. *Cancer Cell* 14:212–225.
16. Lee DF, et al. (2009) KEAP1 E3 ligase-mediated down-regulation of NF-kappaB signaling by targeting IKKbeta. *Mol Cell* 36:131–140.
17. Meylan E, et al. (2009) Requirement for NF-kappaB signalling in a mouse model of lung adenocarcinoma. *Nature* 462:104–107.
18. Xia Y, et al. (2012) Reduced cell proliferation by IKK2 depletion in a mouse lung-cancer model. *Nat Cell Biol* 14:257–265.
19. Gorrini C, Harris IS, Mak TW (2013) Modulation of oxidative stress as an anticancer strategy. *Nat Rev Drug Discov* 12:931–947.
20. Trachootham D, Alexandre J, Huang P (2009) Targeting cancer cells by ROS-mediated mechanisms: A radical therapeutic approach? *Nat Rev Drug Discov* 8:579–591.
21. Vafa O, et al. (2002) c-Myc can induce DNA damage, increase reactive oxygen species, and mitigate p53 function: A mechanism for oncogene-induced genetic instability. *Mol Cell* 9:1031–1044.
22. Shibutani S, Takeshita M, Grollman AP (1991) Insertion of specific bases during DNA synthesis past the oxidation-damaged base 8-oxodG. *Nature* 349:431–434.
23. Satoh H, et al. (2016) NRF2 intensifies host defense systems to prevent lung carcinogenesis, but after tumor initiation accelerates malignant cell growth. *Cancer Res* 76:3088–3096.
24. Hayes JD, McMahon M (2009) NRF2 and KEAP1 mutations: Permanent activation of an adaptive response in cancer. *Trends Biochem Sci* 34:176–188.
25. Zhaorigetu S, Yanaka N, Sasaki M, Watanabe H, Kato N (2003) Silk protein, sericin, suppresses DMBA-TPA-induced mouse skin tumorigenesis by reducing oxidative stress, inflammatory responses and endogenous tumor promoter TNF-alpha. *Oncol Rep* 10:537–543.
26. Park E, et al. (2007) Reduction in IkappaB kinase alpha expression promotes the development of skin papillomas and carcinomas. *Cancer Res* 67:9158–9168.
27. Xu C, et al. (2006) Inhibition of 7,12-dimethylbenz(a)anthracene-induced skin tumorigenesis in C57BL/6 mice by sulforaphane is mediated by nuclear factor E2-related factor 2. *Cancer Res* 66:8293–8296.
28. Long DJ, 2nd, et al. (2000) NAD(P)H:quinone oxidoreductase 1 deficiency increases susceptibility to benzo(a)pyrene-induced mouse skin carcinogenesis. *Cancer Res* 60:5913–5915.
29. Irani K, et al. (1997) Mitogenic signaling mediated by oxidants in Ras-transformed fibroblasts. *Science* 275:1649–1652.
30. Collado M, et al. (2005) Tumour biology: Senescence in premalignant tumours. *Nature* 436:642.
31. Collado M, Serrano M (2010) Senescence in tumours: Evidence from mice and humans. *Nat Rev Cancer* 10:51–57.
32. DuPage M, Dooley AL, Jacks T (2009) Conditional mouse lung cancer models using adenoviral or lentiviral delivery of Cre recombinase. *Nat Protoc* 4:1064–1072.
33. Hu Y, et al. (2001) IKKalpha controls formation of the epidermis independently of NF-kappaB. *Nature* 410:710–714.
34. Zandi E, Rothwarf DM, Delhase M, Hayakawa M, Karin M (1997) The IkappaB kinase complex (IKK) contains two kinase subunits, IKKalpha and IKKbeta, necessary for IkappaB phosphorylation and NF-kappaB activation. *Cell* 91:243–252.
35. Liu B, Chen Y, St Clair DK (2008) ROS and p53: A versatile partnership. *Free Radic Biol Med* 44:1529–1535.
36. Lambeth JD (2004) NOX enzymes and the biology of reactive oxygen. *Nat Rev Immunol* 4:181–189.
37. Panday A, Sahoo MK, Osorio D, Batra S (2015) NADPH oxidases: An overview from structure to innate immunity-associated pathologies. *Cell Mol Immunol* 12:5–23.
38. Pender A, et al. (2015) Efficient genotyping of KRAS mutant non-small cell lung cancer using a multiplexed droplet digital PCR approach. *PLoS One* 10:e0139074.
39. Lund AK, Peterson SL, Timmins GS, Walker MK (2005) Endothelin-1-mediated increase in reactive oxygen species and NADPH oxidase activity in hearts of aryl hydrocarbon receptor (AhR) null mice. *Toxicol Sci* 88:265–273.
40. Suzuki T, Motohashi H, Yamamoto M (2013) Toward clinical application of the Keap1-Nrf2 pathway. *Trends Pharmacol Sci* 34:340–346.
41. Fischle W, Wang Y, Allis CD (2003) Binary switches and modification cassettes in histone biology and beyond. *Nature* 425:475–479.
42. Lehnertz B, et al. (2003) Suv39h-mediated histone H3 lysine 9 methylation directs DNA methylation to major satellite repeats at pericentric heterochromatin. *Curr Biol* 13:1192–1200.
43. Liu K, et al. (2015) NQO1 stabilizes p53 in response to oncogene-induced senescence. *Int J Biol Sci* 11:762–771.
44. Asher G, Lotem J, Cohen B, Sachs L, Shaul Y (2001) Regulation of p53 stability and p53-dependent apoptosis by NADH quinone oxidoreductase 1. *Proc Natl Acad Sci USA* 98:1188–1193.
45. Khan EM, et al. (2006) Epidermal growth factor receptor exposed to oxidative stress undergoes Src- and caveolin-1-dependent perinuclear trafficking. *J Biol Chem* 281:14486–14493.
46. Coant N, et al. (2010) NADPH oxidase 1 modulates WNT and NOTCH1 signaling to control the fate of proliferative progenitor cells in the colon. *Mol Cell Biol* 30:2636–2650.
47. Wang H, et al. (2014) *Porphyromonas gingivalis*-induced reactive oxygen species activate JAK2 and regulate production of inflammatory cytokines through c-Jun. *Infect Immun* 82:4118–4126.
48. Satoh H, Moriguchi T, Takai J, Ebina M, Yamamoto M (2013) Nrf2 prevents initiation but accelerates progression through the Kras signaling pathway during lung carcinogenesis. *Cancer Res* 73:4158–4168.